A Screening Assessment of the Impact of Sedimentological Heterogeneity on CO2 Migration and Stratigraphic-Baffling Potential: Sherwood and Bunter Sandstones, UK

Alshakri, Jafar; Hampson, Gary; Jacquemyn, Carl; Jackson, Matthew; Petrovskyy, Dmytro; Geiger, S.; Silva, Julio Daniel Machado; Judice, Sicilia; Rahman, Fazilatur; Sousa, Mario Costa

A screening assessment of the impact of sedimentological heterogeneity on CO_2 migration and stratigraphic-baffling potential: Sherwood and Bunter sandstones, UK

Jafar Alshakri[1], Gary J. Hampson[1]*, Carl Jacquemyn[1], Matthew D. Jackson[1], Dmytro Petrovskyy[2,3], Sebastian Geiger[2,3], Julio D. Machado Silva[4], Sicilia Judice[4], Fazilatur Rahman[4] and Mario Costa Sousa[4]

[1]Department of Earth Science and Engineering, Imperial College London, London SW7 2AZ, UK

[2]Institute of Geoenergy Engineering, Heriot-Watt University, Edinburgh EH14 4AS, UK

[3]Department of Geoscience and Engineering, Delft University of Technology, 2600 AA Delft, The Netherlands

[4]Department of Computer Science, University of Calgary, Calgary TN2 1N4, Canada

GJH, 0000-0003-2047-8469; CJ, 0000-0002-8627-7144; MDJ, 0000-0002-8276-3575; SG, 0000-0002-3792-1896; SJ, 0000-0001-5621-4196; MCS, 0000-0002-4347-0884
Present addresses: JA, 1st Line Defence, Hertfordshire EN11 0EX, UK
*Correspondence: g.j.hampson@imperial.ac.uk

Abstract: We use a combination of experimental design, sketch-based reservoir modelling and flow diagnostics to rapidly screen the impact of sedimentological heterogeneities that constitute baffles and barriers on CO_2 migration in depleted hydrocarbon reservoirs and saline aquifers of the Sherwood Sandstone Group and Bunter Sandstone Formation, UK. These storage units consist of fluvial sandstones with subordinate aeolian sandstones, floodplain and sabkha heteroliths and lacustrine mudstones. The predominant control on effective horizontal permeability is the lateral continuity of aeolian-sandstone intervals. Effective vertical permeability is controlled by the lateral extent, thickness and abundance of lacustrine-mudstone layers and aeolian-sandstone layers, and the mean lateral extent and mean vertical spacing of carbonate-cemented basal channel lags in fluvial facies-association layers. The baffling effect on CO_2 migration and retention is approximated by the pore volume injected at breakthrough time, which is controlled largely by three heterogeneities, in order of decreasing impact: (1) the lateral continuity of aeolian-sandstone intervals; (2) the lateral extent of lacustrine-mudstone layers; and (3) the thickness and abundance of fluvial-sandstone, aeolian-sandstone, floodplain-and-sabkha-heterolith and lacustrine-mudstone layers. Future effort should be focused on characterizing these three heterogeneities as a precursor for later capillary, dissolution and mineral trapping.

Supplementary material: Rapid Reservoir Modelling prototype (executable and source code) is available at: https://bitbucket.org/rapidreservoirmodelling/rrm. The 32 models used in this study are available at: https://figshare.com/articles/dataset/RRM_models_of_Sherwood_and_Bunter_Sandstones_19210002

The Triassic Sherwood Sandstone Group and lithostratigraphically equivalent Bunter Sandstone Formation are widely considered for large-scale CO_2 storage in saline aquifers and depleted hydrocarbon reservoirs of the onshore and offshore UK, because of their high storage capacity and favourable injectivity (e.g. Kirk 2005; Holloway *et al.* 2006; Heinemann *et al.* 2012; Monaghan *et al.* 2012; Noy *et al.* 2012; Williams *et al.* 2014; Agada *et al.* 2017). Current storage projects under appraisal include depleted Sherwood Sandstone Group hydrocarbon reservoirs in the Hamilton, Hamilton North and Lennox fields of the Liverpool Bay area, East Irish Sea (https://www.eni.com/en-IT/media/press-release/2020/10/carbon-storage-licence-uk.html) and the Bunter Sandstone Formation saline aquifer in the Endurance storage site, southern North Sea (Bentham *et al.* 2017; Gluyas and Bagudu 2020) (Fig. 1). Other hydrocarbon reservoirs in these stratigraphic units also have the potential to be used for future CO_2 storage, including the large Sherwood Sandstone Group reservoir in the Wytch Farm field, southern England (cf. Hogg *et al.* 1999) (Fig. 1).

To date, CO_2 storage characterization and modelling studies of the Sherwood Sandstone Group and Bunter Sandstone Formation have focused largely on storage volumes, aquifer continuity and connectivity and pressurization related to fault seal (e.g. Smith *et al.* 2011; Bricker *et al.* 2012; Noy *et al.* 2012; Williams *et al.* 2013a, 2014; Agada *et al.*
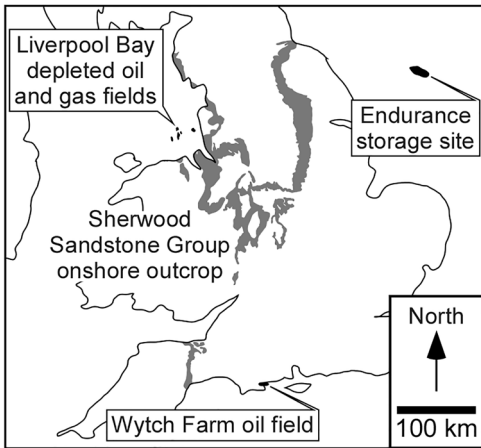
Fig. 1. Map locating Sherwood Sandstone Group outcrops of the onshore UK, offshore CO_2 storage sites currently being appraised in the East Irish Sea and southern North Sea, and the Wytch Farm oil field.

2017; Bentham *et al.* 2017). Assessment of the impact of stratigraphic and sedimentological heterogeneities on CO_2 migration and storage has been limited to: (1) the presence or absence of continuous low-permeability layers, (2) variations in the mean porosity and permeability of specific reservoir facies, (3) the sharp or gradational nature of the contact with the overlying seal and (4) detailed heterogeneity distribution from an outcrop analogue of the contact between the storage unit and seal (Williams *et al.* 2013a, b; Newell and Shariatipour 2016; Onoja and Shariatipour 2018; Onoja *et al.* 2019). These studies demonstrate that stratigraphic and sedimentological heterogeneities can act to disperse the plume of injected CO_2 as it migrates, and can create small-scale stratigraphic trapping configurations that increase CO_2 storage efficiency (cf. Flett *et al.* 2007; Gibson-Poole *et al.* 2009). However, many additional stratigraphic and sedimentological heterogeneities are documented to occur in the Sherwood Sandstone Group and Bunter Sandstone Formation. The relative impact of different heterogeneity types and distributions on CO_2 migration and storage by stratigraphic trapping remains unclear, as does the impact of different stratigraphic and sedimentological architectures in the Sherwood Sandstone Group and Bunter Sandstone Formation (e.g. Medici *et al.* 2015, 2019) on the flow behaviour of CO_2 storage units.

The aim of this paper is to identify the key stratigraphic and sedimentological heterogeneities that control CO_2 migration and stratigraphic baffling in the Sherwood Sandstone Group and Bunter Sandstone Formation. We address this aim using a

screening method that combines experimental design, sketch-based construction of three-dimensional (3D) reservoir models and flow diagnostics. Sketch-based modelling is implemented in open-source research code (Rapid Reservoir Modelling, RRM) that is designed to be geologically intuitive and does not require specialist reservoir modelling experience (Costa Sousa *et al.* 2020; Jacquemyn *et al.* 2021a), and that is integrated with computationally cheap flow diagnostics (Zhang *et al.* 2017, 2020; Jacquemyn *et al.* 2021b; Petrovskyy *et al.* 2022). The method allows a large number of geological scenarios to be explored in a fast, efficient manner prior to more detailed flow simulation.

Geological background

The Sherwood Sandstone Group and Bunter Sandstone Formation both consist of fluvial sandstones with subordinate aeolian sandstones, floodplain and sabkha heteroliths and lacustrine mudstones (e.g. Cooke-Yarborough 1991; Ketter 1991; Meadows and Beach 1993a, b; Ritchie and Pratsides 1993; McKie *et al.* 1998; Meadows 2006; Brookfield 2008; McKie and Williams 2009; Medici *et al.* 2015; Wakefield *et al.* 2015; Newell 2018a, b). The Sherwood Sandstone Group and Bunter Sandstone Formation are overlain by the thick, evaporite-bearing lacustrine mudstones of the Mercia Mudstone Group and Haisborough Group, respectively.

During the Triassic, the UK lay in the eastern, internal part of the Pangaean supercontinent, and occupied a palaeo-latitude of 15–25°N (e.g. Ziegler 1991; McKie and Williams 2009; Newell 2018b). The remnants of the Variscan Mountains lay to the south of the UK, and separated it from the Tethys Ocean. The major river systems that deposited much of the Sherwood Sandstone Group and Bunter Sandstone Formation were derived from the remnants of the Variscan Mountains, and flowed north through a series of linked continental rift basins (McKie and Williams 2009; Tyrrell *et al.* 2012; Morton *et al.* 2013, 2016; Newell 2018b). Additional sediment was supplied by local rivers that drained the flanks of these rift basins (Tyrrell *et al.* 2012; Morton *et al.* 2013, 2016). Aeolian sandstones generally record transport and reworking by westward-directed trade winds (Meadows and Beach 1993a; McKie and Williams 2009; Newell 2018b), and become progressively more common towards the north and west of the UK (e.g. Medici *et al.* 2019). The assemblage of depositional facies in the Sherwood Sandstone Group and Bunter Sandstone Formation is interpreted to record deposition under arid and semi-arid conditions (e.g. Meadows and Beach 1993a, b; McKie *et al.* 1998; Meadows

2006; Brookfield 2008; Medici *et al.* 2015; Wakefield *et al.* 2015). However, facies architecture indicates perennial flow in the major, trunk rivers, implying intense Tethyan-monsoonal precipitation over the remnants of the Variscan Mountains (e.g. McKie and Williams 2009; Medici *et al.* 2015; Newell 2018*a*, *b*). The presence of evaporites, including locally thick halite deposits, in the Mercia Mudstone Group and Haisborough Group, supports deposition in an arid to semi-arid climate. Alternations between fluvial and aeolian deposits, between perennial and ephemeral fluvial deposits and between playa-lacustrine and fluvial deposits are interpreted to record temporal variations between more humid (wetter) and more arid (dryer) climate (e.g. Meadows and Beach 1993*a*; McKie and Williams 2009; Newell 2018*a*). The preservation of these facies-association alternations is influenced locally by tectonic subsidence (e.g. McKie and Williams 2009; Newell 2018*a*).

Sedimentological heterogeneity in the Sherwood Sandstone Group and Bunter Sandstone Formation

We synthesize previous sedimentological studies of the Sherwood Sandstone Group and Bunter Sandstone Formation at outcrop and in the subsurface (Fig. 1) to define a hierarchy of heterogeneity in these units (Fig. 2). This hierarchy is used to define input values for numerical reservoir models in our screening assessment.

At the scale of the sedimentary basins that contain the Sherwood Sandstone Group and Bunter Sandstone Formation, the principal heterogeneity is the interfingering of lithostratigraphic units that comprise fluvial and aeolian sandstones, floodplain and sabkha heteroliths and lacustrine mudstones (Fig. 2a). This interfingering reflects a combination of: tectonic subsidence, which controlled stratal thickness and the distribution of unconformities and related lithostratigraphic units (McKie and Williams 2009; Newell 2018*a*); sediment routing into the basins, which controlled the distribution of trunk river systems and dispersal of the sediment and water that they discharged (Tyrrell *et al.* 2012; Morton *et al.* 2013, 2016; Medici *et al.* 2015); and climatic variations in humidity and aridity, which controlled fluvial discharge and lake extent (Meadows and Beach 1993*a*; McKie and Williams 2009; Newell 2018*a*).

At the scale of individual reservoirs and storage units, basin-scale interfingering of lithostratigraphic units is expressed in the thickness of layers of fluvial sandstones, aeolian sandstones, floodplain and sabkha heteroliths and lacustrine mudstones (Ketter 1991; Meadows and Beach 1993*a*; Ritchie and

Pratsides 1993; Jones and Ambrose 1994; McKie *et al.* 1998; Mountney and Thompson 2002; Meadows 2006; Medici *et al.* 2015; Wakefield *et al.* 2015; Newell 2018*a*) (Fig. 2b). In southerly basins that are proximal to the source of trunk rivers, fluvial sandstone layers are thick and intervening layers of aeolian, floodplain, sabkha and lacustrine deposits are thin and scarce (e.g. in the Wessex Basin of southern England; McKie *et al.* 1998; Newell 2018*a*; Medici *et al.* 2019). In northerly, distal basins, fluvial sandstone layers are thin and intervening layers of aeolian, floodplain, sabkha and lacustrine deposits are thick and abundant (e.g. in the East Irish Sea Basin; Meadows and Beach 1993*a*; Yaliz and Chapman 2003; Meadows 2006; Medici *et al.* 2019). The lateral continuity of aeolian-sandstone and lacustrine-mudstone layers in reservoirs and storage units vary accordingly. For example, aeolian sandstones may occur as laterally continuous sheets or discontinuous lenses (Meadows and Beach 1993*a*; McKie *et al.* 1998; Yaliz and Chapman 2003; Meadows 2006), while lacustrine-mudstone sheets may extend across or pinch out in a reservoir or storage unit (McKie *et al.* 1998; Meadows 2006) (Fig. 2b).

Within reservoirs and storage units, smaller scale heterogeneities occur within layers of fluvial sandstones, aeolian sandstones, floodplain and sabkha heteroliths and lacustrine mudstones (Figs 2b, c & 3). Layers of floodplain and sabkha heteroliths contain channelized fluvial sandbodies and non-channelized sheetflood sandbodies (Ketter 1991; Bowman *et al.* 1993; Meadows and Beach 1993*a*; Ritchie and Pratsides 1993; McKie *et al.* 1998; Medici *et al.* 2015; Newell 2018*a*) (Figs 2b, 3a & d). The proportion of channelized fluvial sandbodies, their connectivity and the geometry and extent of sheetflood sandbodies may all vary in these layers (McKie *et al.* 1998). Fluvial-sandstone layers comprise vertically and laterally stacked channelized fluvial sandbodies, with rare channel-plug mudstones and preserved remnants of floodplain heteroliths (Ketter 1991; Bowman *et al.* 1993; Ritchie and Pratsides 1993; Lorsong and Atkinson 1995; McKie *et al.* 1998; Medici *et al.* 2015; Wakefield *et al.* 2015) (Fig. 2c). Channelized fluvial sandbodies in these layers vary in their preserved dimensions, reflecting differences in river channel mobility and tectonic subsidence rate, and in their internal facies architecture, reflecting differences in river discharge regime and sediment calibre (McKie *et al.* 1998; Medici *et al.* 2015). Thus, heterogeneities in fluvial-sandstone layers include: the abundance, lateral extent and vertical spacing of carbonate-cemented basal channel lags (Dranfield *et al.* 1987; Bowman *et al.* 1993; Lorsong and Atkinson 1995; Newell 2006; Fig. 3a, b); the vertical and lateral succession of facies (e.g. grain-size and sedimentary structures) in each channelized sandbody (Dranfield *et al.* 1987;
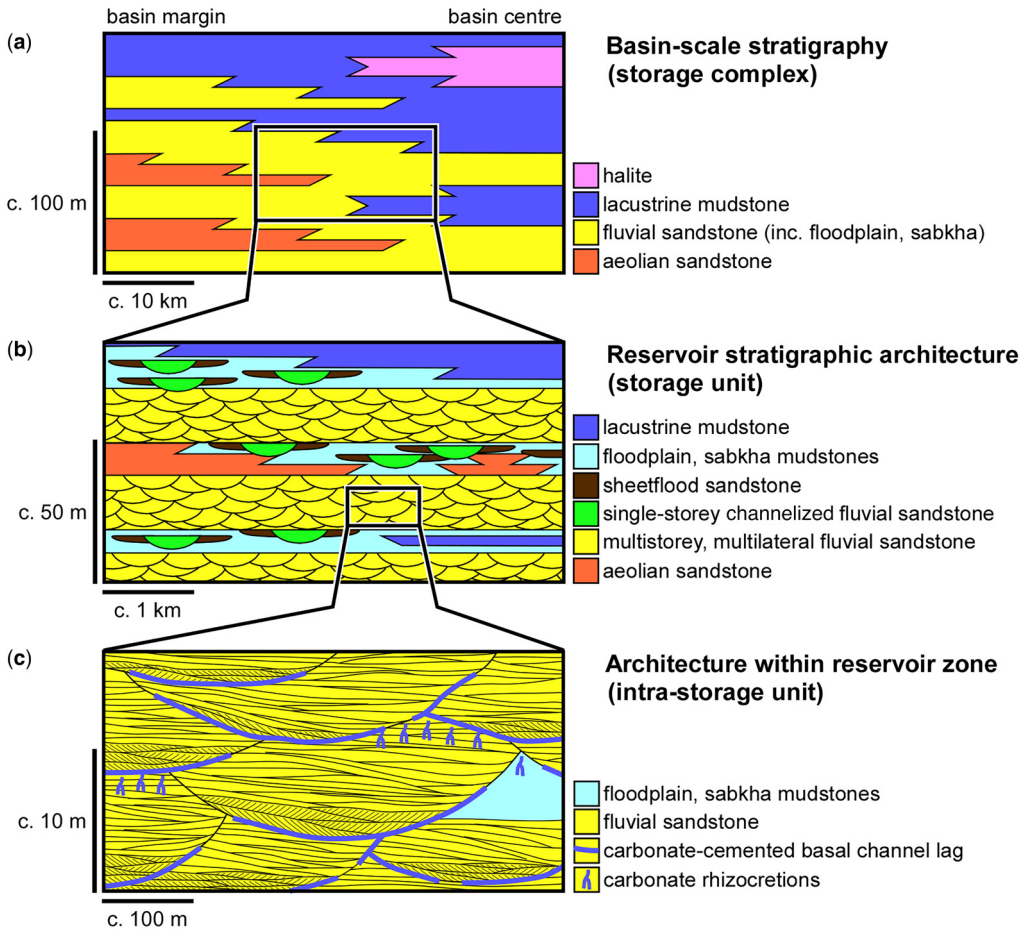
Fig. 2. Interpreted hierarchy of heterogeneities across a range of length scales within the predominantly fluvial and aeolian deposits of the Sherwood Sandstone Group and Bunter Sandstone Formation, and the lacustrine deposits of the overlying Mercia Mudstone Group and Haisborough Group: (**a**) cross-section illustrating basin-scale interfingering of lithostratigraphic units that form the CO_2 storage complex (after McKie and Williams 2009; Newell 2018a, b); (**b**) cross-section illustrating reservoir-scale interfingering of fluvial, aeolian, floodplain/sabkha and lacustrine facies associations that form the CO_2 storage unit (Fig. 3a) (after McKie *et al.* 1998; Yaliz and Chapman 2003; Meadows 2006; Newell 2018a); (**c**) cross-section illustrating stacking of channelized sandbodies within a multistorey fluvial facies association, including carbonate-cemented basal channel lags (Fig. 3a, b) and incompletely preserved channel-fill successions (Fig. 3c) (after Bowman *et al.* 1993; McKie *et al.* 1998; Medici *et al.* 2015; Newell 2018a). Smaller-scale heterogeneities related to facies, sedimentary structures and sandstone texture are not shown.

Ketter 1991; Bowman *et al.* 1993; Lorsong and Atkinson 1995; Medici *et al.* 2015; Wakefield *et al.* 2015; Newell 2018a; Fig. 3b); and the abundance, dimensions and distribution of channel-plug mudstones and preserved remnants of floodplain heteroliths (Dranfield *et al.* 1987; Bowman *et al.* 1993; Lorsong and Atkinson 1995; Medici *et al.* 2015; Fig. 3c) (Fig. 2c). Heterogeneities in aeolian-sandstone layers reflect differences in the stacking of wind-blown sand dunes and their interaction with waterlain, interdune muds and sands (Mountney and Thompson 2002).

Smaller-scale heterogeneities (at centimetre to metre scales) related to sedimentary structures occur within the facies components of channelized fluvial sandbodies, sheetflood sandbodies, aeolian cross-bedded sandstones and other lithological elements. Figure 2 does not portray these heterogeneities. At even smaller scales, sub-centimetre heterogeneities reflect grain-size distributions, sorting and textures together with cementation. Heterogeneities at this scale control porosity, permeability and relative permeability. Aeolian sandstones are better sorted and have lower clay contents than
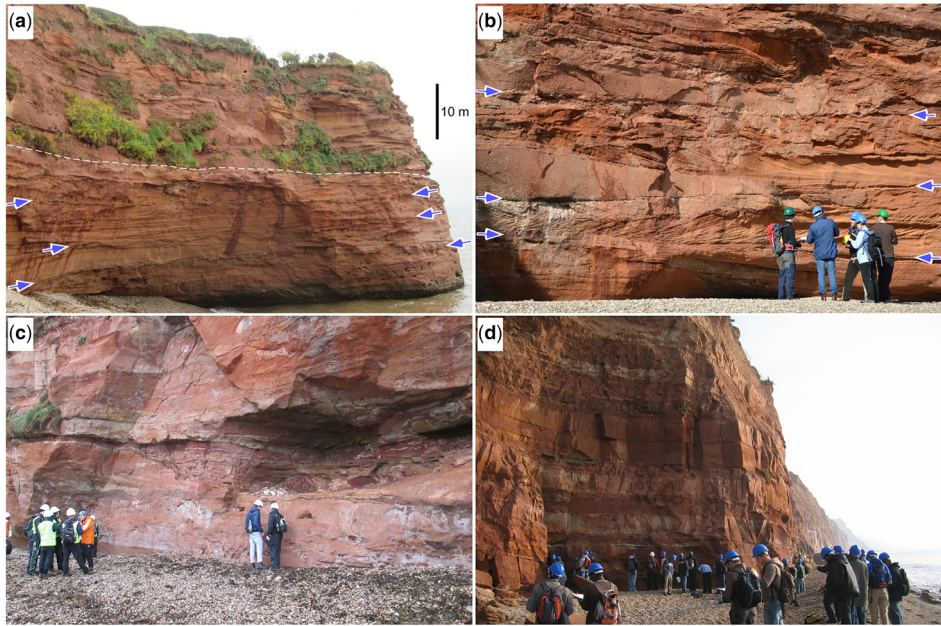
Fig. 3. Photographs of selected heterogeneities in the Sherwood Sandstone Group at outcrop in the south coast of Devon, UK (Fig. 1). (**a**) Fluvial-sandstone layer, characterized by multistorey and multilateral stacking of channelized fluvial sandbodies, overlain (across dotted white line) by layer of floodplain and sabkha heteroliths, which consists of channelized fluvial sandbodies and non-channelized sheetflood sandbodies interbedded with mudstones (Fig. 2b). Resistant, carbonate-cemented lags at the base of channelized fluvial sandbodies (Fig. 2c) are indicated by blue arrows, (**b**) Vertically stacked, partially preserved, channelized fluvial sandbodies in a fluvial-sandstone layer. Each channelized sandbody has a carbonate-cemented lag at its base (indicated by blue arrows), overlain by high-angle cross-beds and then low-angle cross-strata (Fig. 2c), (**c**) Mudstone channel plug in a fluvial-sandstone layer (Fig. 2c), (**d**) Thick, channelized fluvial sandbodies and thin, non-channelized sheetflood sandbodies interbedded with mudstones in a layer of floodplain and sabkha heteroliths (Fig. 2b). Photographs are taken from Ladram Bay (a–c) and Sidmouth East Cliff (d).

fluvial sandstones, and thus are characterized by higher values of porosity and permeability (Meadows and Beach 1993b; Hogg et al. 1996; Bloomfield et al. 2006). Where their grain-size characteristics and texture indicate reworking from aeolian sands, sheetflood sandstones have porosity and permeability values that are intermediate between those of aeolian and fluvial sandstones (Meadows and Beach 1993b); in contrast, sheetflood sandstones have lower porosity and permeability values than fluvial sandstones where their grain-size characteristics and texture indicate reworking and dispersal of fluvially-supplied sand (Hogg et al. 1996). Floodplain and lacustrine mudstones are considered to be non-reservoir lithologies (Ketter 1991; Ritchie and Pratsides 1993; McKie et al. 1998).

Methodology

We use a screening approach to assess the influence of sedimentological heterogeneities that constitute baffles and barriers on CO₂ migration in the Sherwood Sandstone Group and Bunter Sandstone Formation. We do not explicitly model the storage unit at any specific site, but instead investigate the influence of heterogeneities that are generic to all storage sites. We use a method combining three key elements: (1) experimental design, which allows efficient exploration of a wide parameter space; (2) sketch-based reservoir modelling, which enables rapid construction of deterministic models of interpreted geological scenarios; and (3) flow diagnostics, which provide computationally cheap approximations of full-physics, multiphase simulations that are reasonable for many subsurface-flow conditions. These three elements and other aspects of the modelling methods are described below. Integrated sketch-based reservoir modelling and flow diagnostics are implemented in open-source research code (RRM; Zhang et al. 2017, 2020; Costa Sousa et al. 2020; Jacquemyn et al. 2021a, b; Petrovskyy et al. 2022). Our approach is scenario-based and deterministic (Bentley and Smith 2008), and it is

Table 1. *Summary of investigated sedimentological heterogeneities (factors) and their low and high settings in the screening study*

Sedimentological heterogeneity (factor)	Low setting	High setting
thickness of facies-association layers	thin (fluvial: 10 m, aeolian: 5 m, floodplain/sabkha: 5 m, lacustrine: 2 m)	thick (fluvial: 40 m, aeolian: 25 m, floodplain/sabkha: 20 m, lacustrine: 5 m)
lateral continuity of aeolian facies-association bodies	discontinuous lens	continuous sheet
lateral continuity of lacustrine facies-association bodies	discontinuous sheet	continuous sheet
proportion of channelized fluvial sandbodies in floodplain/sabkha facies-association layers	low (*c.* 17%)	high (*c.* 33%)
lateral connectivity of channelized fluvial sandbodies in floodplain/sabkha facies-association layers	isolated clusters of channelized sandbodies	connected network of channelized sandbodies
lateral continuity of sheetflood sandbodies in floodplain/sabkha facies-association layers	continuous sheet	discontinuous lens
mean vertical spacing of carbonate-cemented basal channel lags in fluvial facies-association layers	2 m	10 m
mean lateral extent of carbonate-cemented basal channel lags in fluvial facies-association layers	8 m	20 m

The impact of these eight factors on simulated fluid flow is assessed by observing the percentage change in average response when each factor is varied from its low setting to its high setting.

appropriate for screening the most influential sedimentological heterogeneities prior to more detailed follow-up studies, including stochastic modelling of selected scenarios.

Design of modelling experiment

Based on previous descriptions of the sedimentological character of the Sherwood Sandstone Group and Bunter Sandstone Formation (as synthesized in Fig. 2), we selected eight sedimentological heterogeneities for investigation (Table 1). Established experimental design techniques (Box *et al.* 1978; Damsleth *et al.* 1992; Kjønsvik *et al.* 1994; White and Royer 2003) were used to efficiently explore the resulting parameter space. 256 (i.e. 2^8) modelling scenarios would be developed for all combinations of the eight selected heterogeneities, if each heterogeneity was assigned either a high or low setting, in a full-factorial design. This large number of modelling scenarios is considered to be too time-consuming for a screening assessment. Instead, we used a two-level fractional-factorial design (2_{IV}^{8-3}) in which each factor (heterogeneity) is assigned either a low or high setting. Settings are chosen to represent contrasting, but realistic, values for each

heterogeneity in the various Sherwood Sandstone Group and Bunter Sandstone Formation potential storage units (Table 1). The experimental design allows us to efficiently quantify the effect of varying each factor from its low setting to its high setting. The resolution IV design ensures that the main effects, due to each of the eight studied heterogeneities, are not confounded with interactions between two heterogeneities (Box *et al.* 1978). The experimental design requires only 32 models to be constructed for the screening study (Table 2). This experimental design allows the eight selected heterogeneities to be ranked robustly, based on the average response of a given metric across the ensemble of 32 models. However, additional modelling scenarios would be required to characterize the effects of interactions between two or more heterogeneities, the effects of heterogeneity settings that lie between their high and low settings, and the effects of additional heterogeneities.

Modelled heterogeneities and settings

The eight sedimentological heterogeneities under investigation are listed below in order of decreasing length scale (Fig. 2). Their settings are explained

Table 2. *Design and parameter settings in the 32 models constructed for the screening study*

Sedimentological heterogeneity (factor)	Model number																															
	1	2	3	4	5	6	7	8	9	10	11	12	13	14	15	16	17	18	19	20	21	22	23	24	25	26	27	28	29	30	31	32
thickness of facies-association layers	l	h	l	h	l	h	l	h	l	l	l	l	h	l	h	l	h	l	h	l	h	l	h	l	h	l	h	l	h	l	h	h
lateral continuity of aeolian facies-association bodies	l	l	h	h	l	l	h	h	l	l	l	h	h	l	l	h	h	l	l	h	h	l	l	h	h	l	l	h	h	l	l	h
lateral continuity of lacustrine facies-association bodies	l	l	l	l	h	h	h	h	l	l	l	l	l	h	h	h	h	l	l	l	l	h	h	h	h	l	l	l	l	h	h	h
proportion of channelized fluvial sandbodies in floodplain/sabkha facies-association layers	l	l	l	l	l	l	l	l	l	h	h	h	h	h	h	h	h	l	l	l	l	l	l	l	l	h	h	h	h	h	h	h
lateral connectivity of channelized fluvial sandbodies in floodplain/sabkha facies-association layers	h	h	l	l	l	l	h	h	l	l	h	h	h	h	l	l	l	l	h	h	h	h	l	l	h	h	l	l	l	l	h	h
lateral continuity of sheetflood sandbodies in floodplain/sabkha facies-association layers	l	l	l	l	l	l	l	l	l	l	l	l	l	l	l	l	l	l	h	h	h	h	h	h	h	h	h	h	h	h	h	h
mean vertical spacing of carbonate-cemented basal channel lags in fluvial facies-association layers	l	h	h	l	l	h	h	l	h	l	l	h	h	l	l	h	l	h	h	l	l	h	h	l	h	l	l	h	h	l	l	h
mean lateral extent of carbonate-cemented basal channel lags in fluvial facies-association layers	L	h	h	l	h	l	l	h	l	h	h	l	h	l	l	h	l	h	h	l	h	l	l	h	l	h	h	l	h	l	l	h

l = low, h = high; Table 1.

Sedimentological controls on CO2 migration

below and summarized in Table 2. All models contain a repeated succession of facies-association layers consisting of, from base to top: (1) aeolian sandstone; (2) fluvial sandstone; (3) floodplain and sabkha heteroliths; and (4) capping alternate successions, lacustrine mudstone (Fig. 4). Thus, models contain one layer of lacustrine mudstone for every two layers of fluvial sandstone, aeolian sandstone and floodplain and sabkha heteroliths. The porosity and permeability values assigned to each facies association in the models (Fig. 2b) are listed in Table 3. Absolute values of porosity and permeability differ depending on diagenetic history and burial depth (Burley 1984), but the relative differences between facies associations remain similar (e.g. Meadows and Beach 1993*b*; Hogg *et al.* 1996; Bloomfield *et al.* 2006). We assign lower porosity and permeability values to sheetflood sandstones than to fluvial

sandstones on the assumption that the former were derived from, and are thus finer-grained textural equivalents of, the latter (cf. Hogg *et al.* 1996).

The thickness of facies-association layers (i.e. layers of fluvial sandstones, aeolian sandstones, floodplain and sabkha heteroliths, lacustrine mudstones; Fig. 2b) varies between different Triassic basins that contain storage sites. Fluvial-sandstone layers, consisting of vertically and laterally stacked channelized fluvial sandbodies, form sheets that vary in thickness from 5 to 35 m in the Wessex Basin, including in the Wytch Farm oilfield (McKie *et al.* 1998; Newell 2018*a*), 5 to 40 m in the East Irish Sea Basin, including in the Liverpool Bay oil and gas fields (Meadows and Beach 1993*a*; Yaliz and Chapman 2003; Meadows 2006) and 5 to 65 m in the southern North Sea, including the Caister, Esmond, Forbes and Gordon gas fields
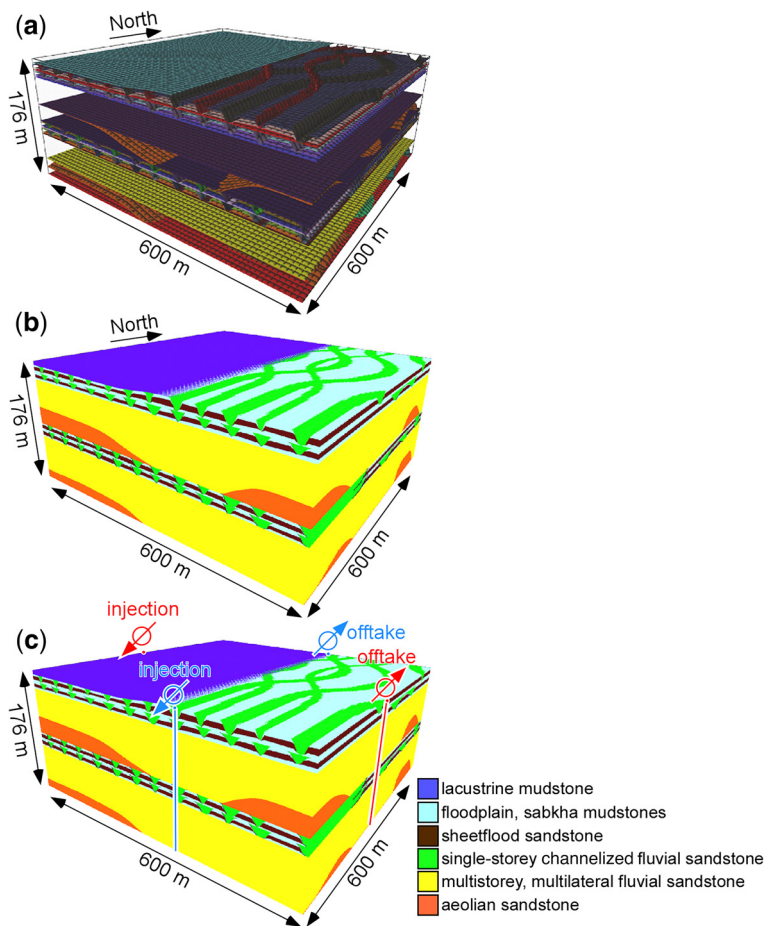

Fig. 4. 3D perspective views of a representative model showing: (**a**) sketch-generated surfaces, (**b**) surface-bounded geological domains and (**c**) well placements for south-to-north tracer flow (blue) and west-to-east tracer flow (red). Model grids are shown for visualization purposes only.

Table 3. *Porosity and permeability values assigned to each facies association represented in the models (Fig. 2b)*

Facies association	Porosity (%)	Permeability (mD)
aeolian sandstone	24	3000
fluvial sandstone	17	500
sheetflood sandstone	15	200
floodplain and sabkha mudstone	5	1
lacustrine mudstone	7	1

(Ketter 1991; Ritchie and Pratsides 1993). Aeolian sandstones occur as discontinuous sheets and lenses up to 15 m thick in the Wessex Basin (McKie *et al.* 1998; Newell 2018*a*), discontinuous sheets 5–30 m thick in the East Irish Sea Basin (Meadows and Beach 1993*a*; Yaliz and Chapman 2003; Meadows 2006) and are absent in the Bunter Sandstone gas fields of the southern North Sea (Ketter 1991; Ritchie and Pratsides 1993). Floodplain and sabkha heteroliths form sheets of varying continuity that are 5–20 m thick in the Wessex Basin (McKie *et al.* 1998; Newell 2018*a*), 5–10 m thick in the East Irish Sea Basin (Meadows and Beach 1993*a*; Yaliz and Chapman 2003; Meadows 2006) and 10–20 m thick in the Bunter Sandstone gas reservoirs of the southern North Sea (Ketter 1991; Ritchie and Pratsides 1993). Lacustrine-mudstone layers occur as thin (<10 m) sheets in all three basins (Ketter 1991; Meadows and Beach 1993*a*; Ritchie and Pratsides 1993; McKie *et al.* 1998; Yaliz and Chapman 2003; Meadows 2006; Newell 2018*a*). Based on these thickness ranges, we select the following values for low and high settings of facies-association layers: 10 and 40 m for fluvial sandstones; 5 and 25 m for aeolian sandstones; 5 and 20 m for floodplain and sabkha heteroliths; and 2 and 5 m for lacustrine mudstones (Table 1). These are not extreme end-member values, but represent values that can occur in potential storage sites in most offshore and onshore UK basins (Fig. 1). We choose to include aeolian sandstones in all our models, even though they are not interpreted in the Bunter Sandstone gas reservoirs of the southern North Sea (Ketter 1991; Ritchie and Pratsides 1993); the latter unit is sparsely sampled by core, so it remains possible that Bunter Sandstone saline aquifers contain aeolian sandstones (Gluyas and Bagudu 2020). Our models all have a uniform thickness (176 m), such that they either contain a small number of thick facies-association layers or a large number of thin facies-association layers (Fig. 5).

The lateral continuity of aeolian-sandstone layers is varied between a low setting of discontinuous lenses of areal extent *c.* 350 × 170 m and a high setting of continuous sheets (Table 1; Figs 2b & 5). These low and high settings are consistent, respectively, with observations from the Wytch Farm oilfield in the Wessex Basin (McKie *et al.* 1998) and the Liverpool Bay oil and gas fields in the East Irish Sea Basin (Meadows and Beach 1993*a*; Yaliz and Chapman 2003; Meadows 2006). The lateral continuity of lacustrine-mudstone layers is also varied between a low setting of discontinuous sheets, representing the marginal pinch-out of a playa lake, and a high setting of continuous sheets (Table 1; Figs 2b & 5). Fluvial-sandstone layers and floodplain-and-sabkha-heterolith layers are represented as continuous sheets in all models (Fig. 5).

The proportion of channelized fluvial sandbodies in floodplain-and-sabkha-heterolith layers (Fig. 2b) is varied between low and high settings of *c.* 17 and 33% (Table 1). Channelized fluvial sandbodies are modelled as single-storey units with widths and thicknesses of *c.* 20 m and *c.* 5–10 m, respectively. The number of these bodies is doubled in models with the high setting, relative to models with the low setting. The connectivity of these channelized fluvial sandbodies is varied by changing their plan-view geometry and spacing, between: (1) several clusters of 2–3 connected channelized sandbodies that are isolated from other clusters in the low setting; and (2) in the high setting, intersecting clusters of 2–3 channelized sandbodies that form a laterally connected network of channelized sandbodies over the entire model area (Table 1). All channelized fluvial sandbodies are modelled as having low sinuosities (1.03–1.15) and uniform widths in plan view. The geometry of sheetflood sandbodies, which also have the potential to connect channelized fluvial sandbodies in floodplain-and-sabkha-heterolith layers (Fig. 2b), is varied between a high setting of discontinuous lenses *c.* 150 m wide and a low setting of continuous sheets (Table 1). In the high setting, lenticular sheetflood sandbodies extend across the width of two channelized fluvial sandbodies that cut into them, and then thin to their lateral pinchouts. The sheetflood sandbodies have straight pinchouts in plan view, and thus maintain a uniform cross-sectional geometry in the third dimension (i.e. parallel to the mean centreline position of the two channelized fluvial sandbodies). In the low setting, sheetflood sandbodies form continuous sheets of approximately uniform thickness that are cut into by all channelized fluvial sandbodies developed at the same stratigraphic level. The proportions, thicknesses and widths of channelized fluvial sandbodies and sheetflood sandbodies for the various settings described above are generally consistent with those documented at outcrop and interpreted in closely spaced wells in the Sherwood Sandstone Group and Bunter Sandstone Formation (e.g. Meadows
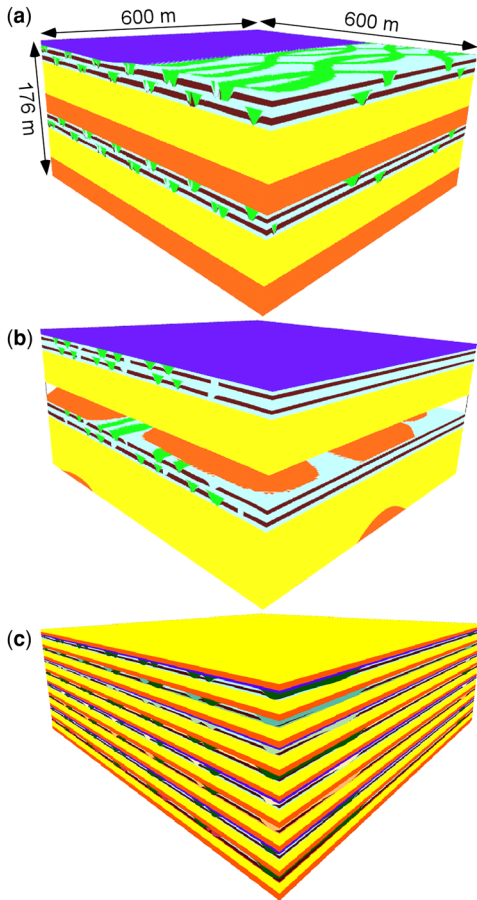
Fig. 5. 3D perspective views of selected models, illustrating contrasting stratigraphic architectures that result from combinations of the settings for different heterogeneities (Table 1): (**a**) model number 28, characterized by thick facies-association layers, laterally continuous aeolian-sandstone sheets, laterally discontinuous lacustrine-mudstone sheets, many and relatively poorly connected channelized fluvial sandbodies and discontinuous sheetflood sandbodies in floodplain-and-sabkha-heterolith layers (Table 2); (**b**) model number 22, characterized by thick facies-association layers, laterally discontinuous aeolian-sandstone lenses, laterally continuous lacustrine-mudstone sheets, few and well connected channelized fluvial sandbodies and discontinuous sheetflood sandbodies in floodplain-and-sabkha-heterolith layers (Table 2); and (**c**) model number 15, characterized by thin facies-association layers, laterally continuous aeolian-sandstone sheets and lacustrine-mudstone sheets, many and relatively poorly connected channelized fluvial sandbodies and continuous sheetflood sandbodies in floodplain-and-sabkha-heterolith layers (Table 2). See Figure 4 for key to facies association colours, but note that channelized fluvial sandbodies in different

and Beach 1993*a*; McKie *et al.* 1998; Medici *et al.* 2015).

In fluvial-sandstone layers, we vary the mean vertical spacing and mean lateral extent of carbonate-cemented lags at the base of channelized fluvial sandbodies (Fig. 2c) in order to reflect variations in the depositional geometry, stacking and preservation of such sandbodies. Outcrops and subsurface cores of the Sherwood Sandstone Group in the Wessex Basin (e.g. Fig. 3a, b) indicate that representative vertical spacing varies between low and high settings of 2 and 10 m, respectively, and representative lateral extent between low and high settings of 8 and 20 m, respectively (Dranfield *et al.* 1987; Bowman *et al.* 1993; Lorsong and Atkinson 1995; Newell 2006; Table 1). More laterally extensive carbonate-cemented basal lags resulting from pronounced multilateral stacking of channelized fluvial sandbodies (Lorsong and Atkinson 1995; Newell 2006) are excluded from our estimates. The low- and high-setting values of mean lateral extent and vertical spacing are used to estimate k_v/k_h ratio using the statistical derivation of Begg and King (1985), also applied by Dranfield *et al.* (1987), and assuming that vertical permeability is equal to horizontal permeability in the intervening sandstones:

$$k_v/k_h = (1 - F_s)/\{1 + s^*(l/3)\}^2 \qquad (1)$$

where F_s is the fraction of cemented lag, s is the inverse of the mean vertical spacing of cemented lags and l is the mean length of cemented lags. F_s is assigned a value of 0.07 (after Bowman *et al.* 1993; Lorsong and Atkinson 1995). The resulting estimates of permeability anisotropy (k_v/k_h ratio) that account for variations in the distribution and extent of carbonate-cemented basal channel lags are: (1) 0.16 for the low settings of both mean vertical spacing and mean lateral extent; (2) 0.05 for the low setting of mean vertical spacing and high setting of mean lateral extent; (3) 0.57 for the high setting of mean vertical spacing and low setting of mean lateral extent; and (4) 0.33 for the high settings of both mean vertical spacing and mean lateral extent. Basal channel lags in the East Irish Sea Basin and southern North Sea are more rarely carbonate-cemented (Ketter 1991; Meadows and Beach 1993*a*; Yaliz and Chapman 2003;

Fig. 5. *Continued*. floodplain-and-sabkha-heterolith layers are assigned different colours in (c), to help with their identification during model construction and quality checking. Fluvial sandstones in between laterally discontinuous aeolian-sandstone lenses are not visualized in (b), so that the geometry of the latter can be seen.

Gluyas and Bagudu 2020), but may contain abundant mudstone clasts that result in low permeabilities (Ketter 1991).

Sketch-based construction of reservoir models

We use an intuitive, sketch-based approach that adapts generic sketch-based interface and modelling (SBIM) methods to construct the reservoir models. In this approach, all geological architectures and heterogeneities (e.g. stratigraphic surfaces, facies-association boundaries, sandbody boundaries) are represented by surfaces that define and bound geological domains (cf. Pyrcz *et al.* 2005; Caumon *et al.* 2009; Sech *et al.* 2009; Ruiu *et al.* 2016; Jacquemyn *et al.* 2019). Since surfaces and surface-bounded geological domains are widely used by geoscientists to conceptualize and represent geological interpretations (e.g. in maps, cross-sections and block diagrams; Fig. 2) and can be generated and manipulated using SBIM methods, with geological viability enforced in the resulting models by operator-controlled interactions between SBIM-generated surfaces, using our sketch-based modelling approach allows non-expert users to capture geological concepts and scenarios (Costa Sousa *et al.* 2020; Jacquemyn *et al.* 2021a).

32 models were constructed, following the experimental design (Table 2). In this study, models were sketched following the hierarchy of heterogeneity (Fig. 2), with heterogeneities at large length scales sketched first, followed by heterogeneities at progressively smaller length scales. Six heterogeneities were sketched explicitly in the models: (1) thickness of facies-association layers; lateral continuity of (2) aeolian and (3) lacustrine facies-association bodies; (4) proportion and (5) connectivity of channelized fluvial sandbodies; and (6) lateral continuity of sheetflood sandbodies in floodplain-and-sabkha facies-association layers (Table 1). Different heterogeneities are sketched in different ways (Costa Sousa *et al.* 2020; Jacquemyn *et al.* 2021a, b). For example, laterally discontinuous lacustrine-mudstone sheets and sheetflood sandbodies (e.g. Figs 4, 5a & b) are sketched in a single vertical cross-section, and their cross-sectional geometry is then extruded linearly into the third dimension. Channelized fluvial sandbodies (Figs 4 & 5a) are sketched in a single vertical cross-section, and their cross-sectional geometry is then extruded along a sketched plan-view trajectory. Laterally discontinuous aeolian-sandstone lenses (Figs 4 & 5b) are constructed by extrapolating between contours sketched on a series of plan-view maps. Where combinations of the same settings for these heterogeneities recur in different models, the surfaces that represent these heterogeneities were re-used in order to maintain consistency in geological-domain geometries and volumes. Two

further heterogeneities, which occur at relatively small length scales, were represented implicitly by assigning different values of permeability anisotropy (k_v/k_h) to geological domains: (7) mean vertical spacing and (8) mean lateral extent of carbonate-cemented basal channel lags in fluvial facies-association layers (Table 1). Since these two heterogeneities are not explicitly represented by sketched surfaces, their setting does not affect geological-domain geometries and volumes.

Each model has dimensions of 600 m (west–east) × 600 m (north–south) × 176 m (thickness) (Fig. 4). The areal extent of the models is thus significantly smaller than that of the Endurance storage site (140 km^2; Gluyas and Bagudu 2020), the Hamilton, Hamilton North and Lennox gas fields (respectively 15, 8 and 9 km^2; Yaliz and Chapman 2003; Yaliz and Taylor 2003) and the Wytch Farm Field (20 km^2; Bowman *et al.* 1993) (Fig. 1). The thickness of the models is comparable to that of the Bunter Sandstone Formation in the Endurance storage site (275 m; Gluyas and Bagudu 2020) and the Sherwood Sandstone Group in the Wytch Farm Field (150 m; McKie *et al.* 1998), although the Sherwood Sandstone Group is considerably thicker in the East Irish Sea Basin (>1000 m; Meadows and Beach 1993a). The models are intended to investigate only a representative part of the potential storage units and sites, at a spatial scale that captures the heterogeneities under investigation. Structural elements of specific storage sites, including faults and tectonic dip, are not incorporated in the models. Depending on the heterogeneity settings for each model, they contain 25–115 geological domains. Models are generated without reference to an underlying grid, although a grid is created to visualize them (Fig. 4) or to perform numerical calculations (Zhang *et al.* 2020).

Architectures modelled in floodplain-and-sabkha-heterolith layers were simplified in three ways, due to practical constraints. (1) Single-storey channelized fluvial sandbodies are narrower (*c.* 20 m; Figs 4 & 5) than those documented at outcrop (*c.* 50 to >75 m; Medici *et al.* 2015; Newell and Shariatipour 2016), in order that we could incorporate variations in sandbody connectivity due to low and high settings of channelized sandbody proportions, channelized sandbody connectivity and sheetflood sandbody continuity in the areal extent of the models (600 × 600 m). (2) Some (but not all) of the channelized fluvial sandbodies developed at a single stratigraphic horizon are sketched with one west-to-east cross-section line and plan-view trajectory, which defines the geometries and lateral spacing of these sandbodies. The other channelized fluvial sandbodies developed at the same stratigraphic horizon are sketched with a second cross-section line and plan-view trajectory. This approach

allows sandbody intersections and connectivity to be defined using only two surfaces, but results in sets of channelized sandbodies that are parallel to each other in plan view (Figs 4 & 5). (3) Discontinuous sheet-flood sandbodies developed at a single stratigraphic horizon are modelled using one west-to-east cross-section line and then extruded linearly in the south-to-north orientation. The resulting sandbodies do not intersect with each other, but do not follow the sinuous plan-view trajectory of the channelized fluvial sandbodies that cut into them. As a result of these three simplifications, details of the modelled architectures in floodplain-and-sabkha-heterolith layers in some models may appear unrealistic; however, the models capture a range of sandstone proportions and sandbody connectivities that are consistent with the interpreted sedimentological scenarios.

Flow diagnostics

Models can be visually inspected to assess that stratigraphic architecture is represented as intended by the user in the sketch-based models (e.g. Fig. 4b). The pore volume of the models can be calculated after porosity values have been assigned to the facies associations in geological domains (Table 3). Flow diagnostics allow key flow properties and behaviours to be assessed by solving a single-phase, steady-state pressure field for a given combination of fluid injection and offtake (production) wells (Shahvali *et al.* 2012; Møyner *et al.* 2014). As a result, tracer flow paths and 'time-of-flight' through connected, highly permeable facies associations are highlighted, and parameters such as effective permeability, Lorenz coefficient, sweep efficiency and storage efficiency can be calculated (Møyner *et al.* 2014). The effects of fluid compressibility, transient flow (e.g. gravity segregation), multiphase fluid interaction (e.g. dissolution) and fluid–rock interactions (e.g. mineralization) are not included in flow diagnostics. We use flow diagnostics to make a rapid, preliminary assessment of the impact of different geological concepts and scenarios on flow properties and behaviours, as a precursor to more detailed but time-consuming full-physics, multiphase simulations (Zhang *et al.* 2017, 2020; Jacquemyn *et al.* 2021b; Petrovskyy *et al.* 2022). A full treatment of our implementation of flow diagnostics is given in Petrovskyy *et al.* (2022).

Volumetric calculations require a grid to be generated for the models, and flow-diagnostic calculations additionally require specification of boundary conditions and the number, location, perforation interval and bottom-hole pressure of injection and offtake wells. An orthogonal grid is used, to ensure numerical stability. Grid cells measure 6.0 m (west–east) × 6.0 m (north–south) × 1.8 m

(thickness), and there are 10^6 grid cells in each model. This grid resolution is sufficiently fine to preserve the geometry and continuity of small geological domains (e.g. single-storey channelized fluvial sandbodies and sheetflood sandbodies; Fig. 4b), and to calculate flow diagnostics with reasonable accuracy, based on sensitivity tests. The faces of each model are set as no-flow boundaries. A single vertical injection well and a single vertical offtake well are placed in the centre of opposing model faces, with both wells perforated over the entire model thickness and the pressure differential between injection and offtake wells set at 50 bar (Fig. 4c). Flow is simulated from south to north (i.e. parallel to the pinchout of lacustrine-mudstone layers, subparallel to the centrelines of sheetflood and channelized fluvial sandbodies in floodplain-and-sabkha-heterolith layers, and along the short axis of aeolian-sandstone lenses; coloured blue in Fig. 4c), and from west to east (i.e. perpendicular to the pinchout of lacustrine-mudstone layers, sub-perpendicular to the centrelines of sheetflood and channelized fluvial sandbodies in floodplain-and-sabkha-heterolith layers and along the long axis of aeolian-sandstone lenses; coloured red in Fig. 4c). These well placements, perforations and bottom-hole pressure constraints are not indicative of the development plan for any storage site, but are instead chosen to investigate fluid migration and potential retention over the length scale of the model volume.

Volumetric and flow-diagnostic calculations for different models are compared using four metrics: (1) total pore volume, which describes the maximum potential for fluid storage; (2) effective permeability, computed for the model volume in three major directions (*x*, *y*, *z*) using flow-based upscaling with no-flow boundaries; (3) Lorenz coefficient, which describes the degree of heterogeneity under dynamic conditions within the storage unit; and (4) pore volume injected at breakthrough time, which provides a measure of how much injected fluid is stored in the model volume as a result of stratigraphic baffling and trapping. The Lorenz coefficient is calculated from the cumulative frequency distributions of mean effective permeability in the *x* and *y* directions (k_x, k_y) in horizontal layers of the models, and varies between 0 for a homogeneous unit and 1 for a completely heterogeneous unit (Schmalz and Rahme 1950). The Lorenz coefficient and pore volume injected at breakthrough time are calculated for both west-to-east and south-to-north tracer flow (coloured red and blue, respectively, in Fig. 4c). Since flow diagnostics are calculated for tracer flow, values of pore volume injected at breakthrough time do not account for residual water saturation; these values are systematic overestimates, but are appropriate as indicative values for screening purposes.

Results

Stratigraphic architectures

Visual inspection of the sketch-based models (e.g. Figs 4b & 5) indicates that modelled stratigraphic architectures are consistent with the geological concepts and data on which they are based (Fig. 2a, b). These modelled architectures reflect the sequence and lateral continuity of facies-association layers together with the proportion, distribution and geometry of sheetflood and channelized fluvial sandbodies in floodplain-and-sabkha-heterolith layers (Table 2).

Total pore volume

Values of total pore volume in the suite of 32 models range from 9.9×10^6 m^3, equivalent to an average porosity of 15.6% (model number 22; Table 2), to 11.0×10^6 m^3, equivalent to an average porosity of 17.3% (model number 11; Table 2), with a mean value of 10.5×10^6 m^3 (equivalent to an average porosity of 16.6%). The lateral continuity of aeolian-sandstone bodies has the largest impact on total pore volume (7%; Fig. 6), because this controls the volume of the most porous facies association (Table 3). The thickness of facies-association layers has the second largest impact (2%; Fig. 6), whereas all other heterogeneities and the confounded interactions of multiple heterogeneities have only a small effect (<1%; Fig. 6). Overall, the total pore volume of the models is relatively uniform.

Effective permeability

Effective permeability at the scale of the model volume is anisotropic. Mean values of effective permeability in the suite of models are 830, 820 and 20 mD in the west–east (k_x), north–south (k_y) and vertical (k_z) orientations, respectively.

The lateral continuity of aeolian-sandstone bodies has by far the largest impact on both k_x and k_y (61 and 66%, respectively; Fig. 7a). Discontinuous aeolian-sandstone lenses (low setting; Table 1) do not extend across the model volume in either a west–east or north–south orientation, in contrast to continuous aeolian-sandstone sheets (high setting; Table 1). The resulting discrepancy in the connectivity between opposing model faces of high-permeability aeolian sandstones accounts for the large effect on k_x and k_y. All other heterogeneities, and the confounded interactions of multiple heterogeneities, have a much smaller effect (<7%; Fig. 7a).

In contrast, multiple heterogeneities control k_z. The two heterogeneities with the largest effects are the lateral continuity of lacustrine mudstones (93%; Fig. 7b) and the thickness of facies-association layers

(76%; Fig. 7b). Both parameters influence the tortuosity of vertical flow paths around low-permeability lacustrine-mudstone and floodplain-mudstone baffles (Table 3), because they control the lateral extent and the number of such baffles. The effects of mean lateral extent and mean vertical spacing of carbonate-cemented channel lags in fluvial-sandstone layers are also influential (47 and 37%; Fig. 7b); these two heterogeneities control vertical flow-path tortuosity in fluvial-sandstone layers (Begg and King 1985). The lateral continuity of aeolian-sandstone bodies has a significant effect (41%; Fig. 7b), as does the proportion of channelized fluvial sandbodies in layers of floodplain-and-sabkha heteroliths (26%; Fig. 7b). Both of these heterogeneities control the number of vertical flow paths through relatively low-permeability layers. The confounded effects of interacting heterogeneities, for example, those of the lateral continuity of lacustrine mudstones in combination with the thickness of facies-association layers, may also be important (up to 48%; Fig. 7b).

Lorenz coefficient

Values of the Lorenz coefficient are similar for south-to-north displacements (mean of 0.40, and range of 0.27–0.50) and west-to-east displacements (mean of 0.42, and range of 0.34–0.50) in the suite of models. The models, therefore, exhibit a similar degree of heterogeneity in north–south and west–east orientations.

The lateral continuity of aeolian-sandstone bodies has the largest impact on the Lorenz coefficient (44 and 25% in north–south and west–east orientations, respectively; Fig. 8), while the thickness of facies-association layers has the second largest impact (8 and 12% in north–south and west–east orientations, respectively; Fig. 8). The effects of other individual heterogeneities and the confounded effects of interacting heterogeneities are minor (<2%; Fig. 8).

Pore volume injected at breakthrough time

Mean values of pore volume injected at breakthrough time are similar for south-to-north displacements (mean of 0.59, and range of 0.49–0.76) and west-to-east displacements (mean of 0.54, and range of 0.44–0.73) in the suite of models. These values provide an indication of the effects of stratigraphic baffling and trapping on CO_2 migration and retention, but they do not correspond directly to values of storage efficiency.

The three individual heterogeneities with the largest impact on pore volume injected at breakthrough time are: (1) the lateral continuity of aeolian-sandstone bodies (29 and 17% in north–south and west–east orientations, respectively;
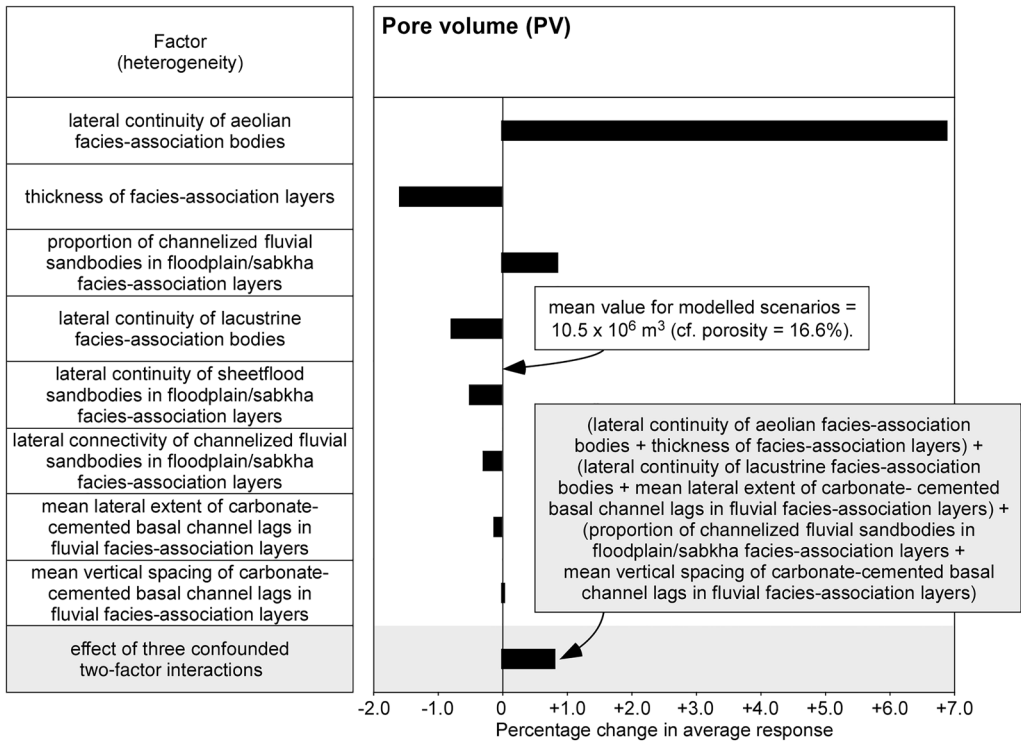
Fig. 6. Tornado chart showing the average percentage changes in total pore volume that result from varying each sedimentological heterogeneity (factor) from its low setting to its high setting (Table 1). If the bar lies to the right then the change is positive. For example, modelling continuous aeolian-sandstone sheets (high setting) increases total pore volume by *c*. 7% compared with modelling discontinuous lenses of aeolian sandstone (low setting). The largest response of confounded two-factor interactions is shown for comparison with the main effects due to individual factors. Changes in total pore volume are small (<7%) for all factors.

Fig. 9); (2) the lateral continuity of lacustrine-mudstone bodies (5 and 9% in north–south and west–east orientations, respectively; Fig. 9); and (3) the thickness of facies-association layers (1 and 13% in north–south and west–east orientations, respectively; Fig. 9). Other individual heterogeneities have small effects in both north–south and west–east orientations (<6%; Fig. 9). The confounded effects of interacting heterogeneities are also significant (up to 7 and 20% in north–south and west–east orientations, respectively; Fig. 9).

Implications for Sherwood and Bunter sandstone storage units and storage sites

Our results indicate that effective permeability (k_x, k_y, k_z), the Lorenz coefficient and pore volume injected at breakthrough time are controlled by three heterogeneities, for the settings chosen in this study (Table 1): (1) the lateral continuity of aeolian-sandstone bodies; (2) the lateral continuity of

lacustrine-mudstone bodies; and (3) the thickness of facies-association layers (Figs 7–9). Preferential flow through thick, high-permeability aeolian sandstones is evident in simulated tracer flow saturations that are visualized at different times (e.g. Fig. 10). In addition, k_z is controlled by the mean lateral extent and mean vertical spacing of carbonate-cemented channel lags in fluvial-sandstone layers (Fig. 7b). These results are consistent with production data from the Sherwood Sandstone Group reservoirs of the Wytch Farm oilfield and the Bunter Sandstone Formation reservoirs of southern North Sea gas fields, in which thin lacustrine mudstones of varying lateral extent act to stratigraphically compartmentalize the reservoirs (Cooke-Yarborough 1991; Ketter 1991; Bowman *et al.* 1993; Hogg *et al.* 1999), and of the East Irish Sea gas fields, in which aeolian-sandstone layers contribute a disproportionately large amount to flow (Cowan 1993). In these various fields, additional heterogeneities due to faults and burial-related diagenesis, which are not investigated in this study, are also important locally in generating
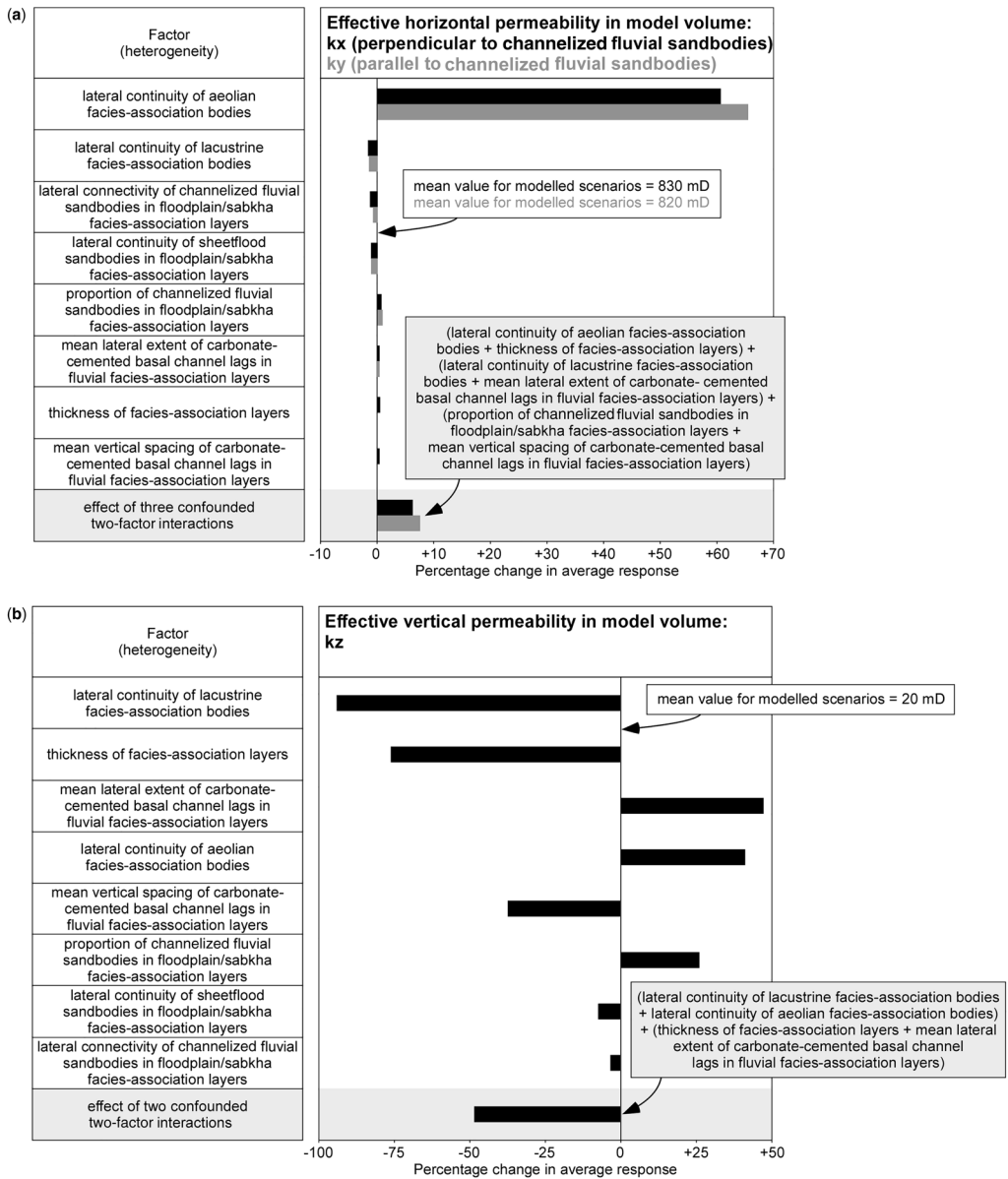
Sedimentological controls on CO₂ migration

Fig. 7. Tornado charts showing the average percentage changes in (**a**) effective horizontal permeability in west–east (k_x) and north–south (k_y) orientations, and (**b**) effective vertical permeability (k_z) that result from varying each factor from its low setting to its high setting (Table 1). If the bar lies to the right then the change is positive. For each tornado chart, the largest response of confounded two-factor interactions is shown for comparison with the main effects due to individual factors.

reservoir compartmentalization, reducing reservoir quality and/or decreasing pressure support and water influx from the aquifer (e.g. Bowman *et al.* 1993; Meadows and Beach 1993*a*; Cooke-Yarborough and Smith 2003).

By implication, the thickness, lateral continuity and distribution of aeolian sandstones and lacustrine mudstones will control CO₂ plume migration in Sherwood Sandstone Group and Bunter Sandstone Formation storage units. The thickness and
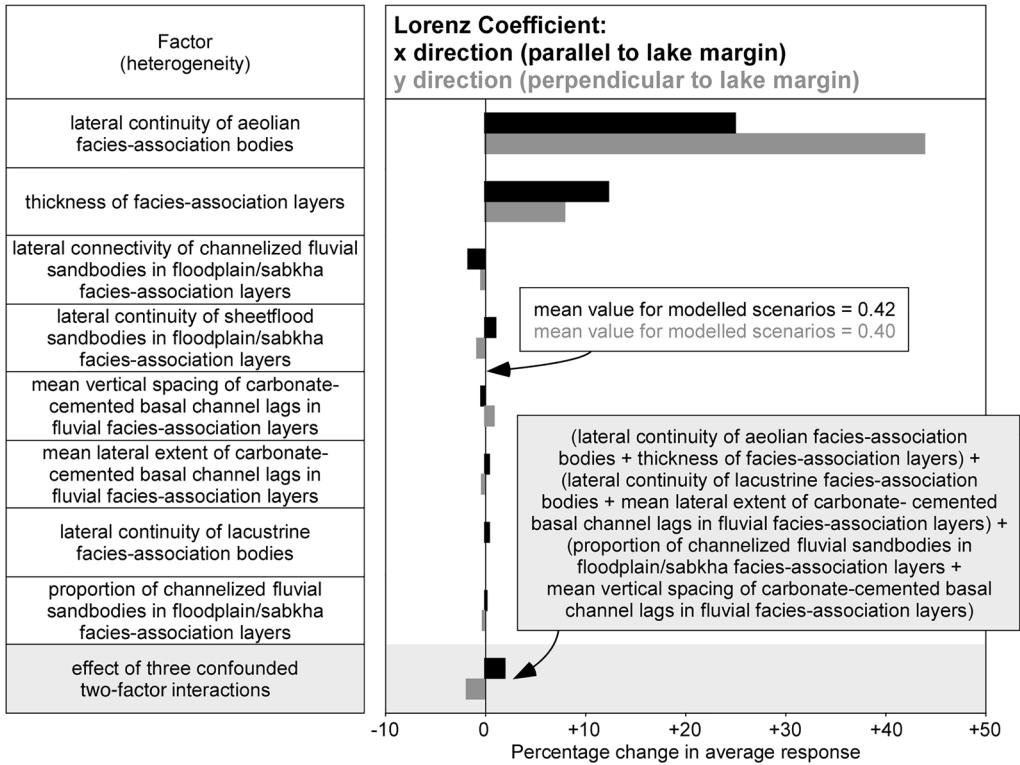
Fig. 8. Tornado chart showing the average percentage changes in Lorenz coefficient that result from varying each factor from its low setting to its high setting (Table 1). If the bar lies to the right then the change is positive. The largest response of confounded two-factor interactions is shown for comparison with the main effects due to individual factors.

stratigraphic position of aeolian-sandstone and lacustrine-mudstone layers can be interpreted from well data, and related to regional changes in climatic aridity during deposition (e.g. Meadows and Beach 1993*a*; McKie and Williams 2009; Newell 2018*a*). In depleted oil and gas reservoirs, the lateral extent and distribution of aeolian-sandstone and lacustrine-mudstone layers is likely to be known with confidence, because wells are closely spaced (e.g. Meadows and Beach 1993*a*; McKie *et al.* 1998; Yaliz and Chapman 2003). In saline aquifers, which are much more sparsely sampled by wells, the lateral extent and distribution of such layers can be inferred with less confidence from regional palaeogeographical reconstructions (e.g. Ziegler 1991; McKie and Williams 2009; Bachmann *et al.* 2010). For example, aeolian sandstones are interpreted to be absent in the Bunter Sandstone Formation reservoirs of southern North Sea gas fields (Cooke-Yarborough 1991; Ketter 1991; Ritchie and Pratsides 1993), but their presence and potential distribution at the Endurance storage site is uncertain (e.g. Gluyas and Bagudu

2020). Similarly, potential pinchout locations of lacustrine shales in the Endurance storage unit are poorly defined. In the Liverpool Bay depleted gas reservoirs, aeolian-sandstone layers are generally continuous across each field (Meadows and Beach 1993*a*; Yaliz and Chapman 2003; Yaliz and Taylor 2003), but may promote rapid lateral plume migration to, and pressure build-up at, faults that seal reservoir compartments. Thus, key sedimentological uncertainties warrant consideration in the development plans of CO_2 storage sites.

Our results suggest that storage units dominated by laterally continuous aeolian-sandstone bodies are likely to be characterized by rapid and isotropic lateral CO_2 migration through these aeolian-sandstone bodies, but slower migration through intervening facies associations (Figs 7a, 8 & 10). Storage units dominated by laterally continuous lacustrine-mudstone bodies are likely to be compartmentalized across these mudstones (Fig. 7b), thus hindering vertical CO_2 migration. Both heterogeneities may thus promote lateral fingering of a CO_2
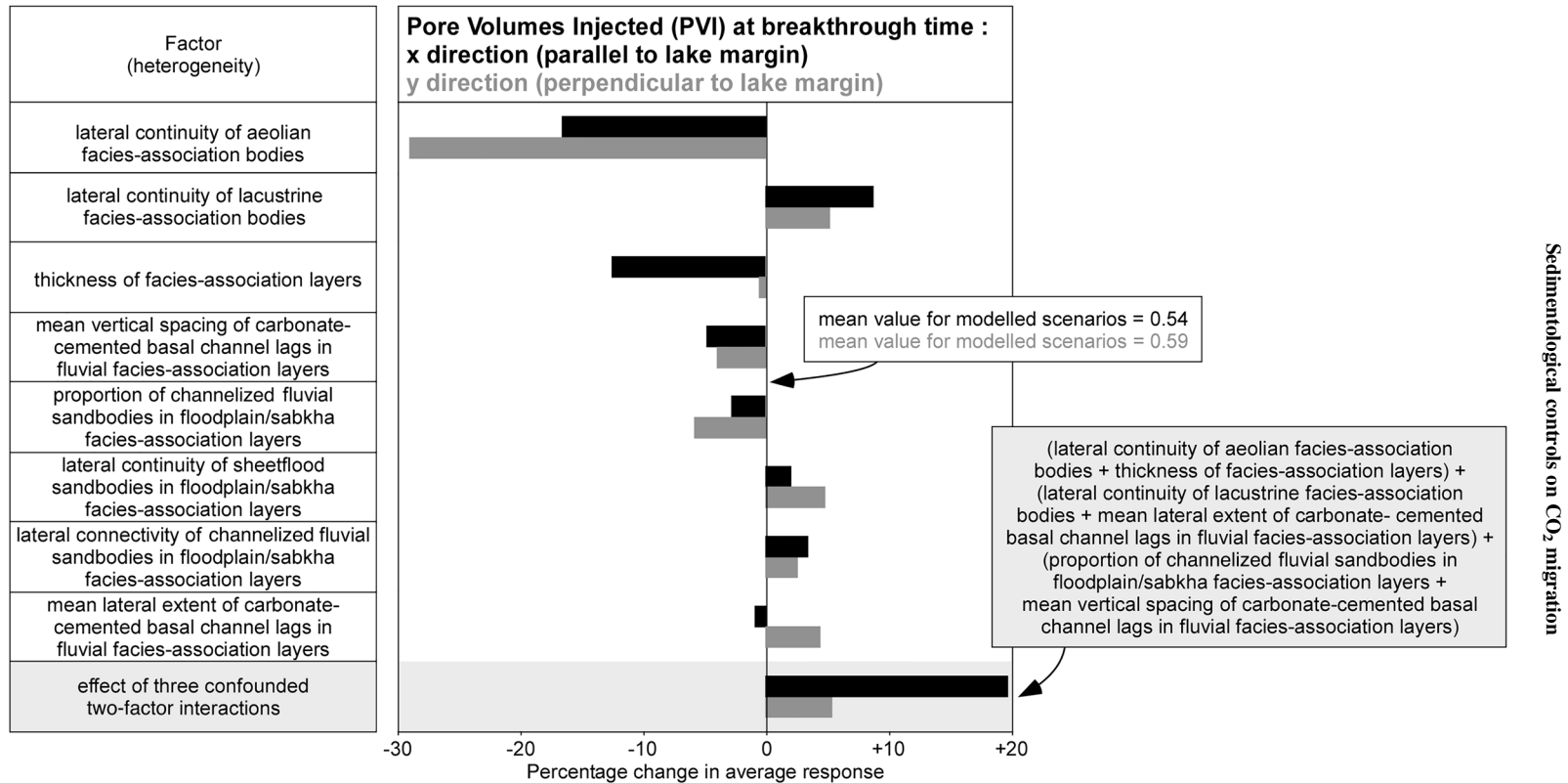
Fig. 9. Tornado chart showing the average percentage changes in pore volume injected at breakthrough time that result from varying each factor from its low setting to its high setting (Table 1). If the bar lies to the right then the change is positive. The largest response of confounded two-factor interactions is shown for comparison with the main effects due to individual factors.
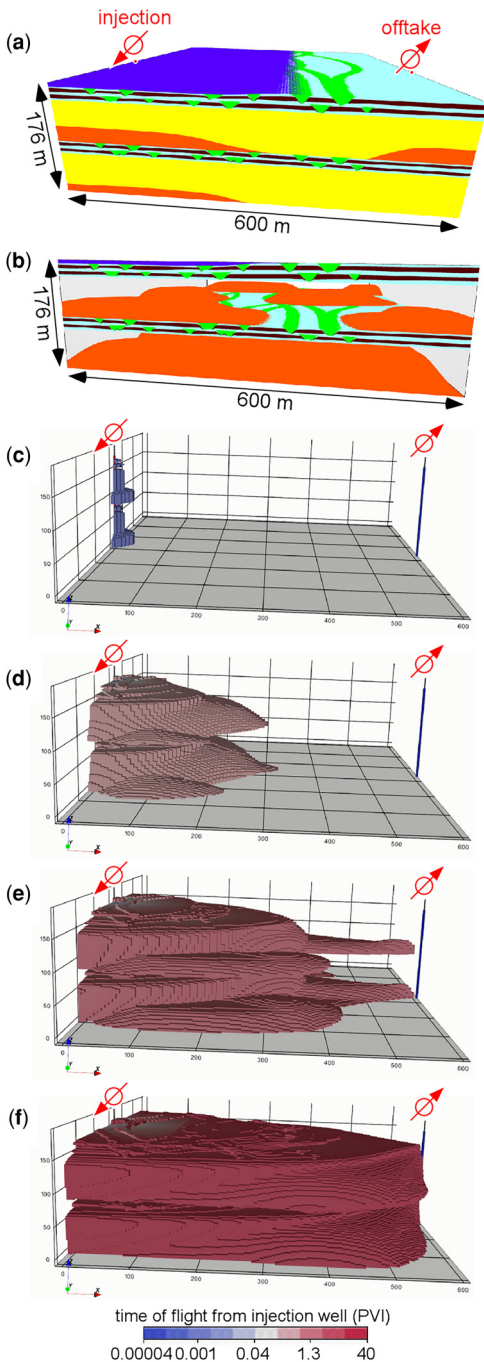
plume, with fingers extending through laterally continuous aeolian sandstones and/or separated by laterally continuous lacustrine mudstones. Such lateral fingering will be accentuated by thin facies-association layers (Figs 7b & 8). The effect of increasing the lateral continuity of lacustrine-mudstone barriers and baffles is to retain CO_2 within the model volume, and thus to increase storage efficiency. In contrast, increasing the lateral continuity of high-permeability, aeolian-sandstone streaks and thief zones results in reduced CO_2 retention within the model volume, thus decreasing storage efficiency in the absence of barriers to lateral flow such as sealing faults.

Conclusions

We assess the impact of sedimentological heterogeneity on CO_2 migration and stratigraphic-baffling and trapping potential in the Sherwood Sandstone Group and Bunter Sandstone Formation, UK using a novel and rapid screening methodology that combines experimental design, sketch-based reservoir modelling and flow diagnostics. Eight heterogeneities were investigated in the screening study: (1) thickness of facies-association layers; lateral continuity of (2) aeolian and (3) lacustrine facies-association bodies; (4) proportion and (5) connectivity of channelized fluvial sandbodies and (6) lateral continuity of sheetflood sandbodies in floodplain-and-sabkha facies-association layers; and (7) mean vertical spacing and (8) mean lateral extent of carbonate-cemented basal channel lags in fluvial facies-association layers. These heterogeneities vary between Sherwood Sandstone Group and Bunter Sandstone Formation storage units at different prospective CO_2 storage sites, or are uncertain within the storage units. Outcrop and subsurface data were used to constrain values of the investigated heterogeneities. Models represent a small part of a CO_2 storage unit, 600×600 m in areal extent and 176 m thick, and lack faults and tectonic dip in order to isolate the effects of sedimentological heterogeneity. Flow was simulated between a single injection and a single offtake well.

Fig. 10. *Continued*. increased durations of time-of-flight from the injector well, (c) Tracer is injected into sheetflood, fluvial and aeolian sandstones, (d) flows preferentially through two laterally discontinuous aeolian sandstones to their eastern pinchouts, (e) breaks through at the offtake well via two more easterly, laterally discontinuous aeolian sandstones and (f) sweeps through remaining aeolian and fluvial sandstones. Tracer breakthrough at the offtake well occurs at 0.45 pore volumes injected (PVI).

Fig. 10. 3D perspective views of model number 2 (Table 2) showing: (**a**) facies-association distributions and well placements for west-to-east tracer flow, (**b**) facies-association distributions with fluvial sandstones not visualized, in order to highlight the geometry and position of laterally discontinuous aeolian sandstones and (**c**–**f**) simulated tracer flow for progressively

The lateral continuity of aeolian-sandstone bodies and lacustrine-mudstone bodies, and the thickness of facies-association layers control effective permeability (k_x, k_y, k_z), the Lorenz coefficient and pore volume injected at breakthrough time (a proxy of the effect of baffles and barriers on CO_2 migration and retention). In addition, k_z is controlled by the mean lateral extent and mean vertical spacing of carbonate-cemented channel lags in fluvial-sandstone layers. Other investigated heterogeneities have only minor influence. These results imply that the distribution and lateral continuity of aeolian sandstones control the direction and rate at which the injected CO_2 plume migrates laterally, while the lateral extent and number of lacustrine-mudstone bodies control vertical plume migration. The effects of these sedimentological heterogeneities should therefore be included in more detailed, future modelling studies of CO_2 migration and storage, particularly where heterogeneity is poorly constrained by well data and hydrocarbon production history in saline aquifers.

Author contributions **JA**: conceptualization (equal), investigation (lead), methodology (equal), writing – original draft (lead), writing – review & editing (supporting); **GJH**: conceptualization (equal), data curation (equal), funding acquisition (equal), methodology (equal), software (supporting), supervision (equal), writing – review & editing (lead); **CJ**: conceptualization (equal), data curation (equal), software (supporting), supervision (equal), writing – review & editing (supporting); **MDJ**: funding acquisition (equal), software (supporting), supervision (equal), writing – review & editing (supporting); **DP**: software (equal), writing – review & editing (supporting); **SG**: funding acquisition (equal), software (supporting), writing – review & editing (supporting); **JDMS**: software (equal), writing – review & editing (supporting); **SJ**: software (equal), writing – review & editing (supporting); **FR**: software (equal),

writing – review & editing (supporting); **MCS**: funding acquisition (equal), software (supporting), writing – review & editing (supporting).

Data availability An open-source version of the software used in model construction has been released (https://bitbucket.org/rapidreservoirmodelling/rrm).

The models constructed for the study are publicly available in a data repository (https://figshare.com/articles/dataset/RRM_models_of_Sherwood_and_Bunter_Sandstones/19210002).

All other data generated or analysed during this study are included in the manuscript.

References

Agada, S., Kolster, C., Williams, G., Vosper, H., MacDowell, N. and Krevor, S. 2017. Sensitivity analysis of the dynamic CO_2 storage capacity estimate for the Bunter Sandstone of the UK southern North Sea. *Energy Procedia*, **114**, 4564–4570, https://doi.org/10.1016/j.egypro.2017.03.1575

Bachmann, G.H., Geluk, M.C. *et al.* 2010. Triassic. *In*: Doornenbal, J.C. and Stevenson, A.G. (eds) *Petroleum Geological Atlas of the Southern Permian Basin Area*. European Association of Geoscientists and Engineers, 149–173.

Bentham, M., Williams, G., Vosper, H., Chadwick, A., Williams, J. and Kirk, K. 2017. Using pressure recovery at a depleted gas field to understand saline aquifer connectivity. *Energy Procedia*, **114**, 2906–2920, https://doi.org/10.1016/j.egypro.2017.03.1418

Begg, S.H. and King, P.R. 1985. Modelling the effects of shales on reservoir performance: calculation of effective vertical permeability. *Paper SPE 13529, presented at the SPE Reservoir Simulation Symposium*, 10–13 February, Dallas.

Bentley, M. and Smith, S. 2008. Scenario-based reservoir modelling: the need for more determinism and less anchoring. *Geological Society, London, Special Publications*, **309**, 145–159, https://doi.org/10.1144/SP309.11

Bloomfield, J.P., Moreau, M.F. and Newell, A.J. 2006. Characterization of permeability distributions in six lithofacies from the Helsby and Wilmslow sandstone formations of the Cheshire Basin, UK. *Geological Society, London, Special Publications*, **263**, 83–101, https://doi.org/10.1144/GSL.SP.2006.263.01.04

Bowman, M.B.J., McClure, N.M. and Wilkinson, D.W. 1993. Wytch Farm oilfield: deterministic reservoir description of the Triassic Sherwood Sandstone.

Geological Society, London, Petroleum Geology Conference Series, **4**, 1513–1517, https://doi.org/10.1144/0041513

Box, G., Hunter, W. and Hunter, J. 1978. *Statistics for experimenters: an introduction to design, data analysis, and model building*. Wiley Press, New York.

Bricker, S.H., Barkwith, A.K.A.P., MacDonald, A.M., Hughes, A.G. and Smith, M. 2012. Effects of CO_2 injection on shallow groundwater resources: a hypothetical case study in the Sherwood Sandstone aquifer, UK. *International Journal of Greenhouse Gas Control*, **11**, 337–348, https://doi.org/10.1016/j.ijggc.2012.09.001

Brookfield, M.E. 2008. Palaeoenvironments and palaeotectonics of the arid to hyperarid intracontinental latest Permian–late Triassic Solway basin (UK). *Sedimentary Geology*, **210**, 27–47, https://doi.org/10.1016/j.sedgeo.2008.06.003

Burley, S.D. 1984. Patterns of diagenesis in the Sherwood Sandstone Group (Triassic), United Kingdom. *Clay Minerals*, **19**, 403–440, https://doi.org/10.1180/claymin.1984.019.3.11

Caumon, G., Collon-Drouaillet, P., Le Carlier de Veslud, C., Viseur, S. and Sausse, J. 2009. Surface-based 3D modeling of geological structures. *Mathematical Geosciences*, **41**, 927–945, https://doi.org/10.1007/s11004-009-9244-2

Cooke-Yarborough, P. 1991. The Hewett field, blocks 48/28-29-30, 52/4a-5a, UK North Sea. *Geological Society, London, Memoirs*, **14**, 433–442, https://doi.org/10.1144/GSL.MEM.1991.014.01.54

Cooke-Yarborough, P. and Smith, P. 2003. The Hewett fields, Blocks 48/28a, 48/29, 48/30, 52/4a, 52/5a, UK North Sea: Hewett, Deborah, Big Dotty, Little Dotty, Della, Dawn and Delilah Fields. *Geological Society, London, Memoirs*, **20**, 731–739, https://doi.org/10.1144/GSL.MEM.2003.020.01.60

Costa Sousa, M., Silva, J.D.M. *et al.* 2020. Smart modelling of geologic stratigraphy concepts using sketches. *Smart Tools and Applications in Computer Graphics (STAG) 2020 Proceedings*, 89–100, https://doi.org/10.2312/stag.20201243

Cowan, G. 1993. Identification and significance of aeolian deposits within the dominantly fluvial Sherwood Sandstone Group of the East Irish Sea Basin UK. *Geological Society, London, Special Publications*, **73**, 231–245, https://doi.org/10.1144/GSL.SP.1993.073.01.14

Damsleth, E., Hage, A. and Volden, R. 1992. Maximum information at minimum cost: a North Sea field development study with an experimental design. *Journal of Petroleum Technology*, **44**, 1350–1360, https://doi.org/10.2118/23139-PA

Dranfield, P., Begg, S.H. and Carter, R.R. 1987. Wytch Farm oilfield: reservoir characterization of the Triassic Sherwood Sandstone for input to reservoir simulation studies. *In*: Brooks, J. and Glennie, K.W. (eds) *Petroleum Geology of Northwest Europe*. Graham & Trotman, London, 149–160.

Flett, M., Gurton, R. and Weir, G. 2007. Heterogeneous saline formations for carbon dioxide disposal: impact of varying heterogeneity on containment and trapping. *Journal of Petroleum Science and Engineering*, **57**, 106–118, https://doi.org/10.1016/j.petrol.2006.08.016

Gibson-Poole, C.M., Svendsen, L., Watson, M.N., Daniel, R.F., Ennis-King, J. and Rigg, A.J. 2009. Understanding stratigraphic heterogeneity: a methodology to maximize the efficiency of the geological storage of CO_2. *American Association of Petroleum Geologists, Studies in Geology*, **59**, 347–364, https://doi.org/10.1306/13171248St593385

Gluyas, J.G. and Bagudu, U. 2020. The Endurance CO_2 storage site, Blocks 42/25 and 43/21, UK North Sea. *Geological Society, London, Memoirs*, **52**, 163–171, https://doi.org/10.1144/M52-2019-47

Heinemann, N., Wilkinson, M., Pickup, G.E., Haszeldine, R.S. and Cutler, N.A. 2012. CO_2 storage in the offshore UK Bunter Sandstone Formation. *International Journal of Greenhouse Gas Control*, **6**, 210–219, https://doi.org/10.1016/j.ijggc.2011.11.002

Hogg, A.J.C., Mitchell, A.W. and Young, S. 1996. Predicting well productivity from grain size analysis and logging while drilling. *Petroleum Geoscience*, **2**, 1–15, https://doi.org/10.1144/petgeo.2.1.1

Hogg, A.J.C., Evans, I.J., Harrison, P.F., Meling, T., Smith, G.S., Thompson, S.D. and Watts, G.F.T. 1999. Reservoir management of the Wytch Farm Oil Field, Dorset, UK: providing options for growth into later field life. *Geological Society, London, Petroleum Geology Conference Series*, **5**, 1157–1172, https://doi.org/10.1144/0051157

Holloway, S., Vincent, C.J., Bentham, M.S. and Kirk, K.L. 2006. Top-down and bottom-up estimates of CO_2 storage capacity in the United Kingdom sector of the southern North Sea basin. *Environmental Geosciences*, **13**, 71–84, https://doi.org/10.1306/eg.11080505015

Jacquemyn, C., Jackson, M.D. and Hampson, G.J. 2019. Surface-based geological reservoir modelling using grid-free NURBS curves and surfaces. *Mathematical Geosciences*, **51**, 1–28, https://doi.org/10.1007/s11004-018-9764-8

Jacquemyn, C., Pataki, M.E.H. *et al.* 2021*a*. Sketch-based interface and modelling of stratigraphy and structure in three dimensions. *Journal of the Geological Society, London*, **178**, jgs2020-187, https://doi.org/10.1144/jgs2020-187

Jacquemyn, C., Hampson, G.J. *et al.* 2021*b*. Rapid reservoir modelling: sketch-based geological modelling with fast flow diagnostics. Paper SPE 208041, presented at the Abu Dhabi International Petroleum Exhibition and Conference (ADIPEC), 15–18 November, Abu Dhabi.

Jones, N.S. and Ambrose, K. 1994. Triassic sandy braidplain and aeolian sedimentation in the Sherwood Sandstone Group of the Sellafield area, west Cumbria. *Proceedings of the Yorkshire Geological Society*, **50**, 61–76, https://doi.org/10.1144/pygs.50.1.61

Ketter, F.J. 1991. The Esmond, Forbes and Gordon fields, blocks 43/8a, 43/13a, 43/15a, 43/20a, UK North Sea. *Geological Society, London, Memoirs*, **14**, 425–432, https://doi.org/10.1144/GSL.MEM.1991.014.01.53

Kirk, K.L. 2005. *Potential for Storage of Carbon Dioxide in the Rocks Beneath the East Irish Sea*. British Geological Survey Internal Report **CR/05/127N**.

Kjønsvik, D., Doyle, J.D., Jacobsen, T. and Jones, A.D.W. 1994. The effects of sedimentary heterogeneities on production from a shallow marine reservoir - what

really matters? Paper SPE 28445, presented at the SPE Annual Technical Conference and Exhibition, 25–28 September, New Orleans.

Lorsong, J.A. and Atkinson, C.D. 1995. *Sedimentology and Stratigraphy of Lower Triassic Alluvial Deposits, East Devon Coast*. Petroleum Group Excursion Guide, Geological Society, London.

McKie, T. and Williams, B. 2009. Triassic palaeogeography and fluvial dispersal across the northwest European Basins. *Geological Journal*, **44**, 711–741, https://doi.org/10.1002/gj.1201

McKie, T., Aggett, J. and Hogg, A.J.C. 1998. Reservoir architecture of the upper Sherwood Sandstone, Wytch Farm field, southern England. *Geological Society, London, Special Publications*, **133**, 399–406, https://doi.org/10.1144/GSL.SP.1998.133.01.21

Meadows, N.S. 2006. The correlation and sequence architecture of the Ormskirk Sandstone Formation in the Triassic Sherwood Sandstone Group of the East Irish Sea Basin, NW England. *Geological Journal*, **41**, 93–122, https://doi.org/10.1002/gj.1034

Meadows, N.S. and Beach, A. 1993*a*. Structural and climatic controls on facies distribution in a mixed fluvial and aeolian reservoir: the Triassic Sherwood Sandstone in the Irish Sea. *Geological Society, London, Special Publications*, **73**, 247–264, https://doi.org/10.1144/GSL.SP.1993.073.01.15

Meadows, N.S. and Beach, A. 1993*b*. Controls on reservoir quality in the Triassic Sherwood Sandstone of the Irish Sea. *Geological Society, London, Petroleum Geology Conference Series*, **4**, 823–833, https://doi.org/10.1144/0040823

Medici, G., Boulesteix, K., Mountney, N.P., West, L.J. and Odling, N.E. 2015. Palaeoenvironment of braided fluvial systems in different tectonic realms of the Triassic Sherwood Sandstone Group, UK. *Sedimentary Geology*, **329**, 188–210, https://doi.org/10.1016/j.sedgeo.2015.09.012

Medici, G., West, L.J. and Mountney, N.P. 2019. Sedimentary flow heterogeneities in the Triassic UK Sherwood Sandstone Group: insights for hydrocarbon exploration. *Geological Journal*, **54**, 1361–1378, https://doi.org/10.1002/gj.3233

Monaghan, A., Ford, J. *et al*. 2012. New insights from 3D geological models at analogue CO₂ storage sites in Lincolnshire and eastern Scotland, UK. *Proceedings of the Yorkshire Geological Society*, **59**, 53–76, https://doi.org/10.1144/pygs.59.1.289

Morton, A., Hounslow, M.W. and Frei, D. 2013. Heavy-mineral, mineral-chemical and zircon-age constraints on the provenance of Triassic sandstones from the Devon coast, southern Britain. *Geologos*, **19**, 67–85, https://doi.org/10.2478/logos-2013-0005

Morton, A., Knox, R. and Frei, D. 2016. Heavy mineral and zircon age constraints on provenance of the Sherwood Sandstone Group (Triassic) in the eastern Wessex Basin, UK. *Proceedings of the Geologists' Association*, **127**, 514–526, https://doi.org/10.1016/j.pgeola.2016.06.001

Mountney, N.P. and Thompson, D.B. 2002. Stratigraphic evolution and preservation of aeolian dune and damp/wet interdune strata: an example from the Triassic Helsby Sandstone Formation, Cheshire Basin, UK. *Sedimentology*, **49**, 805–833, https://doi.org/10.1046/j.1365-3091.2002.00472.x

Møyner, O., Krogstad, S. and Lie, K.A. 2014. The application of flow diagnostics for reservoir management. *SPE Journal*, **20**, 306–323, https://doi.org/10.2118/171557-PA

Newell, A.J. 2006. Calcrete as a source of heterogeneity in Triassic fluvial sandstone aquifers (Otter Sandstone Formation, SW England). *Geological Society, London, Special Publications*, **263**, 119–127, https://doi.org/10.1144/GSL.SP.2006.263.01.06

Newell, A.J. 2018*a*. Evolving stratigraphy of a Middle Triassic fluvial-dominated sheet sandstone: the Otter Sandstone Formation of the Wessex Basin (UK). *Geological Journal*, **53**, 1954–1972, https://doi.org/10.1002/gj.3026

Newell, A.J. 2018*b*. Rifts, rivers and climate recovery: a new model for the Triassic of England. *Proceedings of the Geologists' Association*, **129**, 352–371, https://doi.org/10.1016/j.pgeola.2017.04.001

Newell, A.J. and Shariatipour, S.M. 2016. Linking outcrop analogue with flow simulation to reduce uncertainty in sub-surface carbon capture and storage: an example from the Sherwood Sandstone Group of the Wessex Basin, UK. *Geological Society, London, Special Publications*, **436**, 231–246, https://doi.org/10.1144/SP436.2

Noy, D.J., Holloway, S., Chadwick, R.A., Williams, J.D.O., Hannis, S.A. and Lahann, R.W. 2012. Modelling large-scale carbon dioxide injection into the Bunter Sandstone in the UK Southern North Sea. *International Journal of Greenhouse Gas Control*, **9**, 220–233, https://doi.org/10.1016/j.ijggc.2012.03.011

Onoja, M.U. and Shariatipour, S.M. 2018. The impact of gradational contact at the reservoir-seal interface on geological CO₂ storage capacity and security. *International Journal of Greenhouse Gas Control*, **72**, 1–13, https://doi.org/10.1016/j.ijggc.2018.03.007

Onoja, M.U., Williams, J.D., Vosper, H. and Shariatipour, S.M. 2019. Effect of sedimentary heterogeneities in the sealing formation on predictive analysis of geological CO₂ storage. *International Journal of Greenhouse Gas Control*, **82**, 229–243, https://doi.org/10.1016/j.ijggc.2019.01.013

Petrovskyy, D., Jacquemyn, C.E.M.M. *et al*. 2022. Rapid flow diagnostics for reservoir prototyping - applications to subsurface CO₂ storage. Available at SSRN, http://dx.doi.org/10.2139/ssrn.4207850.

Pyrcz, M.J., Catuneanu, O. and Deutsch, C.V. 2005. Stochastic surface-based modeling of turbidite lobes. *AAPG Bulletin*, **89**, 177–191, https://doi.org/10.1306/09220403112

Ritchie, J.S. and Pratsides, P. 1993. The Caister Fields, Block 44/23s, UK North Sea. *Geological Society, London, Petroleum Geology Conference Series*, **4**, 759–769, https://doi.org/10.1144/0040759

Ruiu, J., Caumon, G. and Viseur, S. 2016. Modeling channel forms and related sedimentary objects using a boundary representation based on non-uniform rational B-splines. *Mathematical Geosciences*, **48**, 259–284, https://doi.org/10.1007/s11004-015-9629-3

Schmalz, J.P. and Rahme, H.D. 1950. The variation of waterflood performance with variation in permeability profile. *Production Monthly*, **15**, 9–12.

Sech, R.P., Jackson, M.D. and Hampson, G.J. 2009. Three-dimensional modeling of a shoreface-shelf parasequence

reservoir analog: part 1. Surface-based modeling to capture high-resolution facies architecture. *American Association of Petroleum Geologists Bulletin*, **93**, 1155–1181, https://doi.org/10.1306/05110 908144

Shahvali, M., Mallison, B., Wei, K. and Gross, H. 2012. An alternative to streamlines for flow diagnostics on structured and unstructured grids. *SPE Journal*, **17**, 768–778, https://doi.org/10.2118/146446-PA

Smith, D.J., Noy, D.J., Holloway, S. and Chadwick, R.A. 2011. The impact of boundary conditions on CO_2 storage capacity estimation in aquifers. *Energy Procedia*, **4**, 4828–4834, https://doi.org/10.1016/j.egypro.2011.02.449

Tyrrell, S., Haughton, P.D., Souders, A.K., Daly, J.S. and Shannon, P.M. 2012. Large-scale, linked drainage systems in the NW European Triassic: insights from the Pb isotopic composition of detrital K-feldspar. *Journal of the Geological Society, London*, **169**, 279–295, https://doi.org/10.1144/0016-76492011-104

Wakefield, O.J., Hough, E. and Peatfield, A.W. 2015. Architectural analysis of a Triassic fluvial system: the Sherwood Sandstone of the East Midlands Shelf, UK. *Sedimentary Geology*, **327**, 1–13, https://doi.org/10.1016/j.sedgeo.2015.07.006

White, C.D. and Royer, S.A. 2003. Experimental design as a framework for reservoir studies. Paper SPE 79676, presented at the SPE Reservoir Simulation Symposium, 3–5 February, Houston.

Williams, J.D.O., Jin, M., Bentham, M., Pickup, G.E., Hannis, S.D. and Mackay, E.J. 2013a. Modelling carbon dioxide storage within closed structures in the UK Bunter Sandstone Formation. *International Journal of Greenhouse Gas Control*, **18**, 38–50, https://doi.org/10.1016/j.ijggc.2013.06.015

Williams, J.D.O., Bentham, M., Jin, M., Pickup, G., Mackay, E., Gammer, D. and Green, A. 2013b. The effect of geological structure and heterogeneity on CO_2 storage in simple 4-way dip structures; a modeling study from the UK Southern North Sea. *Energy Procedia*, **37**, 3980–3988, https://doi.org/10.1016/j.egypro.2013.06.297

Williams, J.D.O., Holloway, S. and Williams, G.A. 2014. Pressure constraints on the CO_2 storage capacity of the saline water-bearing parts of the Bunter Sandstone Formation in the UK Southern North Sea. *Petroleum Geoscience*, **20**, 155–167, https://doi.org/10.1144/petgeo2013-019

Yaliz, A. and Chapman, T. 2003. The Lennox oil and gas field, block 110/15, East Irish Sea. *Geological Society, London, Memoirs*, **20**, 87–96, https://doi.org/10.1144/GSL.MEM.2003.020.01.07

Yaliz, A. and Taylor, P. 2003. The Hamilton and Hamilton North gas fields, block 110/13a, East Irish Sea. *Geological Society, London, Memoirs*, **20**, 77–86, https://doi.org/10.1144/GSL.MEM.2003.020.01.06

Zhang, Z., Geiger, S. *et al.* 2017. A tracing algorithm for flow diagnostics on fully unstructured grids with multipoint flux approximation. *Society of Petroleum Engineers Journal*, **22**, 1946–1962, https://doi.org/10.2118/182635-PA

Zhang, Z., Geiger, S. *et al.* 2020. Fast flow computation methods on unstructured tetrahedral meshes for rapid reservoir modelling. *Computational Geosciences*, **24**, 641–661, https://doi.org/10.1007/s10596-019-09851-6

Ziegler, P.A. 1991. *Geological Atlas of Western and Central Europe*. Shell Internationale Petroleum Maatschappij B.V., The Hague.